Effect Mechanism of Plain Woven Structure of Carbon Fiber on CFRP Cutting

Guojun Dong
Harbin Institute of Technology
Fei Su (sfeihe@163.com)
Hunan University of Science and Technology
Chunjie Li
Hunan University of Science and Technology
Lei Zhen
Yancheng Institute of Technology
Bing Chen
Hunan University of Science and Technology

Research Article

Keywords: Carbon fiber-reinforced plastic (CFRP), plain-woven structure, cutting mechanism, FEM modeling

Posted Date: October 4th, 2021

DOI: https://doi.org/10.21203/rs.3.rs-939156/v1

Version of Record: A version of this preprint was published at The International Journal of Advanced Manufacturing Technology on January 6th, 2022. See the published version at https://doi.org/10.1007/s00170-021-08470-9.

Abstract

Carbon fiber-reinforced plastic (CFRP) is increasingly employed as structural components for aircrafts in aerospace. The plain woven CFRP is more commonly used than the UD-CFRP. The machining-induced damages are easy to occur. The influence of the plain-woven structure on the cutting mechanism and the defects occurrence mechanism are seldom studied in detail. In this paper, the three-dimensional FEM model of plain woven CFRP is established. The occurrence and propagation of the delamination are investigated. The results indicate that the stress concentrations are easy to occur at the junction of warp and fill bundles near the cutting position. The plain-woven structure can block the transfer of stress and the crack propagation. When θ=90°, the damages of the fill fibers and the crack of the interface are easy to occur. When θ=45°, the step-like fracture is formed in both of the warp and the fill bundles, especially in the fill bundles. Under the same cutting conditions, the exit delamination of the plain-woven CFRP is obviously less than that of the UD-CFRP. The delamination greatly increases with the increase of the feed speed. The delamination decreases with the increase of the cutting speed. The delamination is closely related to the instantaneous cutting position of the cutter.

1 Introduction

Carbon fiber-reinforced plastic (CFRP) is increasingly employed as structural components for aircrafts in aerospace due to the good properties, such as high specific strength, high specific stiffness and high modulus [1–5]. Specifically, the plain woven CFRP is more commonly used than the UD-CFRP. In reality, subsequent machining operations, such as milling, drilling, are necessary to be required for the removal of excess material to meet tolerances or for assembling [6]. However, the presence of the machining-induced damages, for example, delamination, cracking, fiber pull-out, etc., let to the poor quality of the machined surface.

Numerous existing studies have investigated the cutting mechanism of CFRP. Alessandro et al. [7–8] pointed out that the cutting mechanism was highly dependent on the fiber orientation and the damage area was orthogonal to the fiber orientation when θ = 135° by the FE cutting model. Su et al. [9] also established a three-dimensional finite element model and characterized the fiber fracture evolution processes of fiber and resin. Meng et al. [10] indicated that the machined surface roughness and the sub-damage could be affected by the fiber orientation by the three-dimension micro-scale cutting simulation model. Cepero-Mejias et al. [11] investigated the influence of cutting parameters on the machining-induced damage of unidirectional (UD) CFRP by establishing the finite element model. Li et al. [12] discussed the damage behaviors of UD-CFRP in single- and multiple-pass strategies orthogonal cutting by combining the FE models and the experiments. Liu et al. [13] proposed a novel three-phase finite element model of CFRP to simulate the machining damages. Cheng et al. [14] revealed the deformation mechanism of UD-CFRP by building the micro-scale thermal-mechanical coupling numerical simulation model. Most of the above researches had only studied the cutting mechanism of the UD-CFRP.

Kishore et al. [15] conducted the drilling experiments for plain weave CFRP. They pointed out that the modulation-assisted drilling technique produces better quality holes than conventional drilling under identical conditions. Voss et al. [16] investigated the occurrence of top layer delamination for the unidirectional CFRP. Hintze et al. [17–18] also studied the occurrence and propagation of the UD-CFRP top ply delamination. An analytical model of maximum fiber protrusion lengths of curved contours was derived. They confirmed that the fiber protrusions could be avoided if the cutting velocity and the cutting edge were appropriately employed. He et al. [19] conducted the slot milling of the UD-CFRP tests. The patterns of cutting force and defects were investigated. They reported that the occurrence of the delamination of UD-CFRP was closely related to fiber cutting angle. In order to deeply investigate the forming mechanism of the delamination, the corrections between weave induced fiber undulation and delamination were investigated. Hintze et al. [20] established a theoretical model for maximum fiber protrusion. They validated that combination of fiber undulation angle and thicknesses of top matrix layer were responsible for different occurrences of delamination. Ghafarizadeh et al. [21] claimed that the machining damage around the cutting area were caused by the fiber compression damage and matrix cracking. Li et al. [22] expounded the occurrence and propagation of fiber burrs and surface cavities for plain woven CFRP. They highlighted that various surface defects predominantly occurred owing to the cutting conditions and fiber configurations, and the defects were mainly located in the layers with fibers orientated at 45°/135°.

Most of the previous researches focus their attention on the cutting mechanism and the delamination of UD-CFRP. However, the cutting mechanism and the defects occurrence mechanism of plain woven CFRP are seldom studied in detail. Especially, the three-dimensional FEM model for plain woven CFRP is extremely rare. In this paper, the three-dimensional FEM model of plain woven CFRP was established. Then, the influence of the plain woven structure on the cutting mechanism was analyzed. The occurrence and propagation of the top layer defects were investigated.

2 Plain-woven Structure And Fe Modelling

2.1 Plain-woven structure and 3D geometrical model

A warp or a fill bundle contains a lot of carbon fibers, as shown in Fig. 1. The fiber bundles have the geometric characteristics of plain-woven structure. To obtain the geometric characteristics of plain-woven CFRP, the necessary assumptions are required. The periodic bending of a bundle is assumed as the cosine curve. The cross-section shape of the bundle is like a convex lens shape and keeps the shape in direction of the bundle. The bundle is the continuum and the volume fraction is basically equal to that of the whole CFRP plate. The warp bundle and the fill bundle have the same bending and cross-section shapes. Taking the fill bundle as the example, the coordinate system *oxy* is established. Then, the two-dimensional contour curves characteristics of a warp bundle can be written by Eq. (1) [23].

$$y = P_1 \cos(P_2 x) + P_3 \quad (1)$$

Where, $P_1 = a/2$ is the amplitude of the bending curve in y direction, a is the thickness of the bundle cross-section center, $P_2 = \pi/b$, b is the distance between two adjacent warp bundles, P_3 is the offset distance of the bending curve in y direction. A straight segment of a warp bundle can be determined by Eq. (2) [23].

$$P_1 \cos(P_2 x) + P_3 \le y \le P_1 \cos(P_2 x) + P_3 + P_4 \quad (2)$$

Where, the range value of x can be determined by the distance b and the width of the cross-section c. $P_4 = d$ is the thickness of the cross-section edge. The relevant characteristic parameters of the geometric shapes can be obtained by observing the plain-woven CFRP. Namely, $a = 0.5$ mm, $b = 2.5$ mm, $c = 2.5$ mm, $d = 0.626$ mm. the warp and the fill bundle can be assumed as a homogeneous equivalent fiber based on the volume fraction, according to the principle of homogenization, the geometric shape characteristic parameters and bending shape function. Then, according to the mechanical mixing law of composite materials, the mechanical properties of a bundle can be expressed as Eq. (3). The 3-dimensional (3D) geometric model of the plain-woven CFRP is established by assembling the warp and fill bundles into a plain-woven model. Simultaneously, in order to approximately simulate the cutting process of plain-woven CFRP as much as possible, a layer of resin matrix is attached to the upper and the lower surface respectively, as illustrated in Fig. 1.

$$\begin{cases} E_1 = E_f c_f + E_m c_m \\ E_2 = \dfrac{E_f E_m}{E_f c_m + E_m c_f} \\ \nu_{21} = \nu_f c_f + \nu_m c_m \\ \nu_{12} = \dfrac{E_2}{E_1}\nu_{21} \\ G_{12} = \dfrac{G_m G_f}{G_f c_m + G_m c_f} \end{cases} \quad (3)$$

Where, E_f, E_m, c_f, c_m, G_f, G_m, ν_f, ν_m, E_1, E_2, G_{12}, ν_{12}, ν_{21} are the Young's elastic modulus of the fiber, the Young's elastic modulus of the matrix, the fiber volume fraction, the matrix volume fraction, the fiber shear modulus, the matrix shear modulus, the fiber Poisson's ratio, the matrix Poisson's ratio, the equivalent elastic modulus in 1-direction (viz. the fiber axial direction), the equivalent elastic modulus in 2-direction (viz. vertical the fiber axial direction), the in-plane shear modulus, the equivalent Poisson's ratio for the deformation in 2-direction causing by the stress in 1-direction, the equivalent Poisson's ratio for the deformation in 1-direction causing by the stress in 2-direction, respectively.

2.2 Cutting finite element modeling of plain-woven CFRP

In order to analyze and compare the plain-woven fibers cutting process, the micro-scale orthogonal cutting simulations with two warp fiber orientation, i.e. $\theta = 45°$ and $\theta = 90°$, are established. When the bundle of fibers is perpendicular to the cutting direction, the bundle of fibers can be defined as the warp. The warp fiber orientation θ is the angle between the warp and the cutting direction, as illustrated in Fig. 2.

Based on the single 3D geometric model of the plain-woven CFRP, the upper and lower layers of resin matrix are regarded as a whole, respectively. The zero thickness elements are built between the resin matrix and the fiber bundle as well as between each bundles of warp and fill. The relevant definitions for various materials for cutting model are listed as follows. 1) The constitutive relation of carbon fiber bundle is implemented into the finite element code through VUMAT to predict the character and the extent of damage. The maximum stress failure criterion is employed to evaluate the removing of the carbon fiber bundle. During the finite element calculation process, if the axial maximum principal stress meets the ultimate tensile strength (X_t) or the minimum principal stress reaches the ultimate compressive strength (X_c), the carbon fiber bundle elements will be deleted, the stress-strain relationship of the carbon fiber bundle is illustrated in Fig. 2. 2) The epoxy matrix in the plain-woven CFRP model is modeled as an isotropic material. The constitutive model is depicted in Fig. 2. The segment AB is the response curve of the material without failure. Once the stress reaches the ultimate tensile or compressive strength at point B, the initial damage is assumed to take place. Point B is the initial failure point. Segment BC is damage evolution curve. The shear failure criterion is used as initial failure criterion. 3) The states of bonding between fiber bundle and epoxy matrix as well as between fiber bundles are assumed as the interface material, namely, the zero thickness elements. To resolve the issue of excessive distortion and stress transfer within a zero thickness element, the cohesion elements are applied. The constitutive response is presented in Fig. 2.

Additionally, the underside and back side of the plain-woven CFRP plate are completely fixed. The contact type between fiber and matrix is considered as the general contact with a friction coefficient of 0.3. A surface-to-surface kinematic contact algorithm is defined to model the interaction between the cutter and the matrix as well the fiber bundle. The normal behavior is defined as hard contact, the tangential behavior is simulated by penalty function, with the friction coefficients of 0.3 and 0.8, respectively. The cutter is modeled as a rigid body and 3-node triangular facet rigid body elements are applied. The fiber bundles are meshed as the hexahedral units (C3D8R) along the fiber axis by using an advanced algorithm. The matrix is meshed as the tetrahedral units (C3D4). The junction or boundary of warp and fill bundles is marked as the symbol of W, as shown in Fig. 2. Thus, a three-dimensional orthogonal cutting model of plain-woven CFRP is established.

3 Experimental Verification

3.1 Experimental details

To validate the finite element simulation model established in the previous sections and analyze the formation mechanisms of the machined surface and delamination, a series of drilling tests were carried out on KVC1050M vertical machining center with coolant, by the novel drill made of YG6X carbide without coating, with 2 flutes and a diameter 6 mm. The drilling parameters of 2000 ~ 5000 rpm in spindle speed and 105 ~ 420 mm/min in feed speed were applied. All the experimental setups were depicted in Fig. 3. After the tests, the microstructures of hole wall were observed and analyzed by scanning electron microscope (SEM). The hole exit were observed and the exit delamination was investigated by ultra-field microsystem. The exit delaminations with different warp fiber orientation were measured, as illustrated in Fig. 4.

The plain woven carbon fiber reinforced plastics (CFRP) with about 10 ~ 15 mm thickness were employed in all these experiments. The fibre diameter was about 7 ~ 8 μm. The fiber volume content was about 60 ~ 70%. Each ply had a thickness of 0.25 mm. The width of a fibers bundle was 2.5 mm. The material properties of CFRP and tool were listed in Table 1.

Table 1
Properties of plain-woven CFRP and cutter

Parameter	Value
Fiber elastic modulus	E_1 = 235 Gpa, $E_2 = E_3$ = 14 GPa
Fiber Poisson ratio	$v_{12} = v_{13}$ = 0.2, v_{23} = 0.25
Fiber shear modulus	$G_{12} = G_{13}$ = 28 Gpa, G_{23} = 5.5 GPa
Fiber tensile strength	X_t=3.59 GPa
Fiber compressive strength	X_c=3 GPa
Matrix elastic modulus	E = 2.96 GPa
Matrix Poisson ratio	v = 0.4
Matrix yield strength	σ_{y0} = 74.4 MPa
Interface properties	t0 n = 60 Mpa, t0 s = t0 t = 110 Mpa Gc n = 0.33 (N/mm^2), Gs c = Gc t = 1.209 (N/mm^2) K_{nn}=4·10^6 (N/mm^2), K_{ss}=K_{tt}=1·10^6 (N/mm^2)
Cutter rake angle	20°
Cutter clearance angle	5°
Cutter blunt round radius	20 μm

4 Results And Discussion

4.1 Influence of plain-woven structure on material removal mechanism

The cutting process of the plain-woven fibers with specified fiber orientations (θ = 90°, 45°, etc.) is analyzed, as presented in Fig. 5 (a)–(b). And the formation mechanisms of cutting surface are studied, as displayed in Fig. 6 (a)–(b).

In Fig. 5 (a), when θ = 90°, the warp and fill fibers are bent and deformed when the cutter pushes forward. The stress concentrations occur at the junction of warp and fill bundles near the cutting position. The stress on the both sides of the warp bundle is slightly larger. And the stress concentration line is basically consistent with the boundary of the warp and the fill. The near the cutting position side of the warp is loaded the tensile stress (as the point I_1). The compressive stress is loaded on the other side of the warp (as the point J_1). Then, the crack firstly occurs on the side of the warp near the cutting position. Subsequently, the cracks develop on the other side. Finally, the brittle fracture develops along the crack on the side of the warp near the cutting position. The fiber fracture is neat. The buckling deformation of the fill bundle is impeded because the deformation of the bundles front the cutter is small owing to the plain-woven structure. The stress concentrations also occur at the junction of warp and fill bundles near the cutting position. As a result, the greater compressive stress is loaded on the fill bundle at the front of cutter (as the point Q), while the tensile stress is loaded on the fill bundle at the back of cutter (as the point H). The initial crack occurs on the fill bundle at the back of cutter, and then the tensile fracture is firstly developed on the fill bundle at the back of cutter. Subsequently, the compression fracture occurs on the fill bundle at the front of cutter. As view of the cutting process, the cutting damage of the fill bundle is more serious than that of the warp bundle.

In Fig. 5 (b), when θ = 45°, the bundles are squeezed and bent. Similarly, the stress concentrations occur at the junction of warp and fill bundles near the cutting position. The near the cutting position side of the warp is loaded the tensile stress (as the point I_2). The compressive stress is loaded on the other side of the warp (as the point J_2). And the initial compression crack occurs on the point I_2. Then, the brittle fracture is extended from the point I_2 as the cutter continues to move forward. In the same way, the stress concentrations occur on the two sides of the fill bundles (as the points I_3 and J_3). The tensile stress is loaded on the point I_3, and then the tensile fracture is extended from this position. The compression stress is loaded on the point J_3, and then the compression fracture is developed from this position. The cracks are mainly concentrated at the junction of warp and fill bundles. Obviously, the stress transfer and the crack propagation are prevented by the junction structure of warp and the fill bundles. Therefore, the junction structure of warp and the fill bundles plays a significant role in preventing the crack propagation and the stress transfer.

The cutting stress zone is mainly concentrated on the front cutter during the cutting of the plain-woven CFRP, as depicted in Figs. 6 (a)–(b). Under the same cutting conditions, the cutting stress zone when θ = 45° is larger than that when θ = 90°. The fibers bundles at the front cutter and the rake face of the cutter are crushed serious. The fibers and the matrix are all crushed. When θ = 90°, the warp fibers are damaged to some extent. However, the significant stress concentration can be observed on the sides of the fill bundles and the interface between the fill bundle and the matrix. The damages of the fill fibers and the crack of the interface can be obviously observed by the SEM observation. The warp fibers fractures are neat, but the fibers roots are broken. When θ = 45°, the step-like fracture is formed in both of the warp and the fill bundles, especially in the fill bundles. These results are basically consistent with the experimental results.

In summary, when θ = 90°, the tensile fracture occurs on the near the cutting position side of the warp bundle and compression fracture appears on the other side of the warp bundle. The warp fibers fractures are neat. The compression fracture occurs on the fill bundle at the front of cutter and the tensile fracture develops on the fill bundle at the back of cutter. The damages of the fill fibers and the crack of the interface are easy to occur. When θ = 45°, the failure of the warp bundles is mainly compression fracture, the failure of the near the cutting position side of the fill bundle is the tensile fracture and the other side is the compression fracture. The step-like fracture is formed in both of the warp and the fill bundles, especially in the fill bundles. Additionally, the stress concentrations are easy to occur at the junction of warp and fill bundles near the cutting position. Then, the plain-woven structure can block the transfer of stress and the crack propagation.

4.2 Influence of plain-woven structure on machining defects

Actually, the basic morphology and the formation mechanism of the delamination of the exit hole can be reflected by the cutting simulation of the plain-woven CFRP. As mentioned above, under the same cutting conditions, the cutting stress zone when θ = 45° is larger than that when θ = 90°. Then, the cutting damage when θ = 90° is less than that when θ = 45°. Therefore, in most cases, the exit delamination when θ = 45° is more serious, as presented in Fig. 7 (a). Furthermore, under the same cutting conditions, the exit delamination of the plain-woven CFRP is obviously less than that of the UD-CFRP due to the blocking effect of the plain-woven structure on the transfer of stress and the crack propagation. Generally, the exit delamination of the UD-CFRP extends along the axial direction of the fiber, as depicted in Fig. 7 (b).

4.3 Influence of processing parameters on effect of plain-woven structure

In order to further investigate the formation and evolution of the exit delamination, according to the finite element cutting model, the influences of the cutting speed and the cutting position on the cutting damages and the exit delamination, as illustrated in Figs. 8 (a)–(b). The cutting damage decreases gradually with the increase of the cutting speed, according to the observation of the cutting damage evolution process when θ = 90° and θ = 45°. When θ = 90°, the cutting damage decreases from 1.8 mm to 0.8 mm as the cutting speed V_c increases from 56.59 mm/min to 69.85 mm/min. And when θ = 45°, the

cutting damage decreases from 3.1 mm to 2.2 mm. During the cutting of the plain-woven CFRP, the cutting position can be divided into two cases. The first case is that the cutter cuts plain-woven CFRP along the middle of a single fill bundle. The other case is that the cutter cuts along the boundary of warp and fill bundles. As revealed above, the stress concentrations are easy to occur at the junction of warp and fill bundles near the cutting position. Then, the plain-woven structure can block the transfer of stress and the crack propagation. Therefore, when the cutting position is at the junction of warp and fill bundles, the cutting damages propagation can be prevented at the junction of warp and fill bundles, and then the cutting damages can be decreased obviously. However, the cutting position is in the middle of a single fill bundle, the cutting damages can't be blocked, but the damages extend to the boundary of warp and fill bundles. When $\theta = 90°$, the cutting damage of warp bundle is less than that of fill bundle. Additionally, the size of the cutting damage is basically equal to the width of the uncut part of the fill bundle. When $\theta = 45°$, the cutting damage of warp bundle is a little less than that of fill bundle. The cutting damage size is approximately equal to the distance between the uncut part of the fill bundle and the junction of warp and fill. Therefore, the larger the width of the uncut parts of the fill bundle, the greater the cutting damage. Namely, the farther the cutting position is from the junction of warp and fill bundle, the greater the cutting damage.

The exit delamination increases with the increase of the feed speed. When spindle speed $n = 4000$ rpm, the feed speed V_f increases from 105 mm/min to 420 mm/min, the average value of exit delamination increases from 3.06 mm to 3.43 mm as $\theta = 90°$, and the average value of exit delamination increases from 3.19 mm to 3.32 mm as $\theta = 45°$. Conversely, the exit delamination slightly reduces with the increase of the spindle speed (or the cutting speed). When the feed speed V_f=315 mm/min, the spindle speed n increases from 2000 rpm to 5000 rpm, the average value of exit delamination decreases from 3.30 mm to 3.22 mm as $\theta = 90°$, and the average value of exit delamination increases from 3.23 mm to 3.13 mm as $\theta = 45°$.

Additionally, the exit delamination size is also closely related to the cutting position of the cutter, as shown in Fig. 10. The tool drills the CFRP. Then, the cutter cuts the CFRP counterclockwise. When the cutter cuts the CFRP from $\theta = 90°$ to $\theta = 45°$, namely the A_1 stage, the cutting position of the cutter is in the middle of a fill bundle. As reported above, under the same cutting condition, the cutting damages when $\theta = 45°$ are slightly larger than that when $\theta = 90°$. Thus, the cutting position is far away from the junction of warp and fill bundle when the cutter cuts plain-woven CFRP from $\theta = 90°$ to $\theta = 45°$. The plain-woven structure is less able to prevent delamination. Therefore, the delamination increases when the cutter cuts plain-woven CFRP from $\theta = 90°$ to $\theta = 45°$. Nevertheless, when the cutting position is close to the junction of warp and fill bundle, the extension of the delamination is inhibited and the delamination gradually decreases, as C_1 and E_1 stages. However, when the cutter cuts plain-woven CFRP from $\theta = 45°$ to $\theta = 90°$, the delamination decreases. Especially, when the cutting position is close to the junction of warp and fill bundle, the propagation of delamination is greatly inhibited due to the plain-woven structure and the delamination is well restrained. Conversely, when the cutting position is far away to the junction of warp and fill bundle, the propagation of delamination can't be prevented until the delamination extends

to the warp and fill junction. The further the cutting position is from the junction, the greater the delamination, as B_1, D_1 and F_1 stages.

In summary, both of cutting speed and feed speed has significant influence on delamination. The delamination greatly increases with the increase of the feed speed. And the delamination decreases with the increase of the cutting speed. Additionally, the delamination is closely related to the instantaneous cutting position of the cutter. When the cutter cuts plain-woven CFRP from $\theta = 90°$ to $\theta = 45°$, the delamination increases because the cutting position is in the middle of a fill bundle. But the delamination can be restrained at the junction of warp and fill bundle. When the cutter cuts plain-woven CFRP from $\theta = 45°$ to $\theta = 90°$, the farther the cutting position is from the warp and fill junction, the greater the delamination is. The delamination maximum value is almost equal to the width of the uncut part of the fill bundle.

5 Conclusions

In this paper, the three-dimensional FEM model of plain-woven CFRP is established. Then, the influence of the plain-woven structure on the cutting mechanism is analyzed. The occurrence and propagation of the top layer delamination are investigated. Some key conclusions are drawn from the results presented in this research as follows:

(1) When $\theta = 90°$, the tensile fracture occurs on the near the cutting position side of the warp bundle and compression fracture appears on the other side of the warp bundle. The damages of the fill fibers and the crack of the interface are easy to occur. When $\theta = 45°$, the failure of the warp bundles is mainly compression fracture, the failure of the near the cutting position side of the fill bundle is the tensile fracture and the other side is the compression fracture. The step-like fracture is formed in both of the warp and the fill bundles, especially in the fill bundles.

(2) The stress concentrations are easy to occur at the junction of warp and fill bundles near the cutting position. Then, the plain-woven structure can block the transfer of stress and the crack propagation.

(3) The exit delamination when $\theta = 90°$ is less than that when $\theta = 45°$. Under the same cutting conditions, the exit delamination of the plain-woven CFRP is obviously less than that of the UD-CFRP.

(4) The delamination greatly increases with the increase of the feed speed. The delamination decreases with the increase of the cutting speed. The delamination is closely related to the instantaneous cutting position of the cutter.

(5) When the cutter cuts plain-woven CFRP from $\theta = 90°$ to $\theta = 45°$, the delamination increases. And the delamination can be restrained at the junction of warp and fill bundle. When the cutter cuts plain-woven CFRP from $\theta = 45°$ to $\theta = 90°$, the farther the cutting position is from the warp and fill junction, the greater the delamination is. The delamination maximum value is almost equal to the width of the uncut part of the fill bundle.

Declarations

Author contribution Guojun Dong: Modeling analysis, test operation, writing-review and editing (Section 4). Fei Su: Conceptualization, formal analysis, resources, writing-review and editing, supervision, project administration, funding acquisition. Chunjie Li: Methodology, validation, investigation, data curation, writing original draft. Lei Zhen: Data curation, writing-review and editing (Section2.3). Bing Chen: Test operation, Matlab programming.

Funding This work was financially supported by the National Science Foundation of China (No.52175400, No.51805164, No.52075127), Natural Science Foundation of Hunan Province (No. 2021JJ30263) and Natural Science Foundation of Jiangsu Province (No.BK20201474)

Data availability All data generated or analyzed during this study are included in this published article.

Ethics approval Authors have read the “Ethical Responsibilities of Authors” and “Compliance with Ethical Standards.” This study is an original paper which has neither previously nor simultaneously in whole or in part been submitted anywhere else. Results are presented clearly, honestly, and without fabrication, falsification, or inappropriate data manipulation. Complied fully with the COPE guidelines.

Consent to participate Not applicable.

Consent for publication Not applicable.

Competing interests The authors declare no competing interests.

References

1. Choudhury M R, Srinivas M S, Debnath K (2018) Experimental investigations on drilling of lignocellulosic fiber reinforced composite laminates. J Manuf Process 34:51-61

2. Zhu Z, Guo K, Sun J, Li J, Liu Y, Zheng Y, Chen L (2018) Evaluation of novel tool geometries in dry drilling aluminium 2024-T351/titanium Ti6Al4V stack. J Mater Process Tech 259:270-281

3. Wang X, Shen X, Zeng C, Sun F (2018) Combined influences of tool shape and as-deposited diamond film on cutting performance of drills for CFRP machining. Surf Coat Tech 347:390-397

4. Loja M A R, Alves M S F, Bragança I M F, Rosa R S B, Barbosa I C J, Barbosa J I (2018) An assessment of thermally influenced and delamination-induced regions by composites drilling. Compos Struct 202:413-423

5. Xu J, Li C, Mi S, An Q, Chen M (2018) Study of drilling-induced defects for CFRP composites using new criteria. Compos Struct 201:1076-1087

6. Deng H, Xu Z (2019) Dressing methods of superabrasive grinding wheels: A review. J Manuf Process 45:46–69

7. Alessandro A, Khamis E (2019) 3D micro-mechanical modelling of orthogonal cutting of UD-CFRP using smoothed particle hydrodynamics and finite element methods. Compos Struct 218:174-193

8. Alessandro A, Sein L S, Khamis E (2017) Modelling the orthogonal cutting of UN-CFRP composites: Development of a novel cohesive zone model. Compos Struct 168:65-83

9. Su Y L (2019) Effect of the cutting speed on the cutting mechanism in machining CFRP. Compos Struct 220:662-676

10 Meng Q X, Cai J Cheng H, Zhang K F (2020) Investigation of CFRP cutting mechanism variation and the induced effects on cutting response and damage distribution. Int J Adv Manuf Technol 106:2893-2907

11 Cepero-mejias F, Curiel-sosa J L, Zhang C, Phadnis V A (2019) Effect of cutter geometry on machining induced damage in orthogonal cutting of UD polymer composites: FE study. Compos Struct 214: 439-450

12 Li H N, Wang J P, Wu C Q, Zhao Y J, Xu J, Liu X L, Zhu W Q (2020) Damage behaviors of unidirectional CFRP in orthogonal cutting: A comparison between single- and multiple-pass strategies. Compos part B 185: 1-13

13 Liu H T, Lin J, Sun Y Z, Zhang J Y (2019) Micro model of carbon fiber/cyanate ester composites and analysis of machining damage mechanism. Chin J Mech Eng 32, 52:1-11

14 Cheng H, Gao J Y, Kafka O L, Zhang K F, Luo B, Liu W K (2017) A micro-scale cutting model for UD CFRP composites with thermo-mechanical coupling. Compos Sci Tech 153: 18-31

15 Kisshore D, Inderdeep S (2017) Low-frequency modulation-assisted drilling of carbon-epoxy composite laminates. J Manuf Process 25: 262-273

16 Voss R, Seeholzer L, Kuster F, Wegener K (2017) Influence of fiber orientation, tool geometry and process parameters on surface quality in milling of CFRP. CIRP J Manuf Sci Tech 18: 75-91

17 Hintze W, Hartmann D, Schutte C (2011) Occurrence and propagation of delamination during the machining of carbon fiber reinforced plastics (CFRPs) – An experimental study. Compos Sci Tech 71: 1719-1725

18 Hintze W, Brugmann F (2018) Influence of spatial tool inclination on delamination when milling CFRP. J Mater Process Tech 252:830-837

19 He Y L, Qing H A, Zhang S G, Wang D Z, Zhu S W (2017) The cutting force and defect analysis in milling of carbon fiber-reinforced polymer (CFRP) composite. Int J Adv Manuf Tech 93: 1829-1842

20 Hintze W, Cordes M, Koerkel G (2015) Influence of weave structure on delamination when milling CFRP. J Mater Process Tech 216: 199-205

21 Ghafarizadeh S, Chatelain J F, Lebrun G (2016) Finite element analysis of surface milling of carbon fiber-reinforced composites. Int J Adv Manuf Tech 87: 399-409

22 Li M J, Huang M J, Jiang X G, Kuo C L, Yang X J (2018) Study on burr occurrence and surface integrity during slot milling of multidirectional and plain woven CFRPs. Int J Adv Manuf Tech 97: 163-173

23 Wang D N, Li J L, Jiao Y N (2013) 3D meso-geometrical model of plain weave fabric and finite element modeling under ballistic impact. J Mater Eng 9: 69-78

Figures

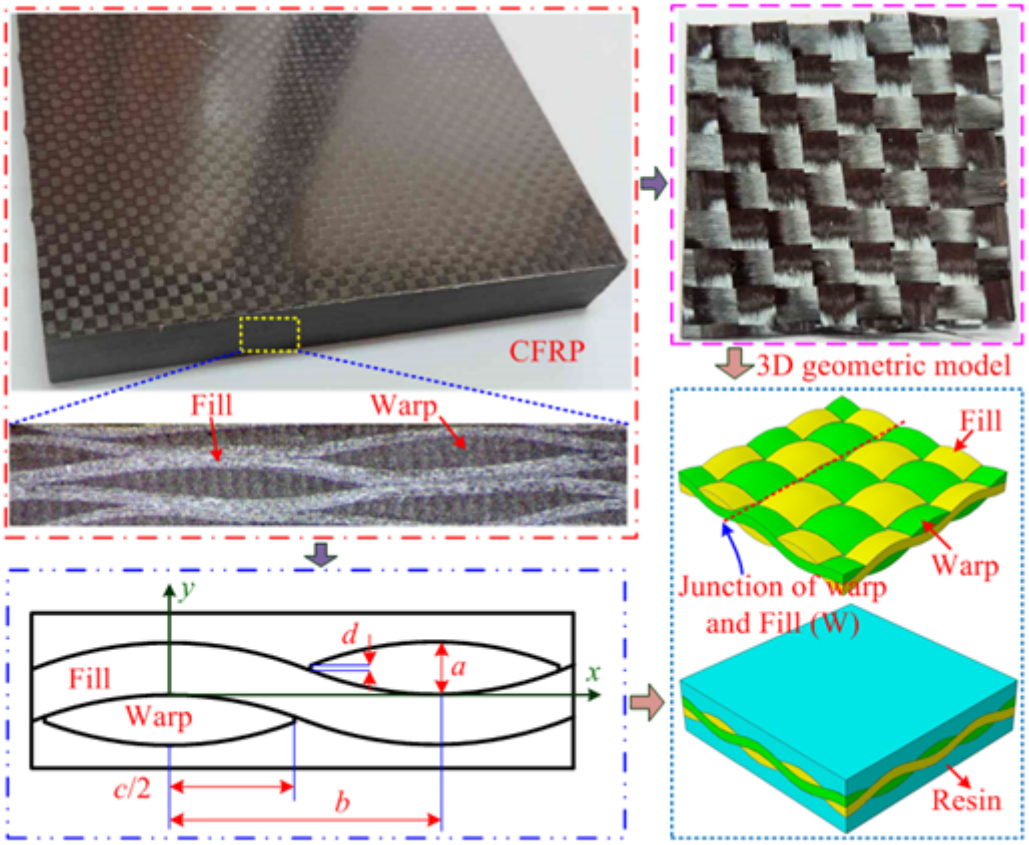

Figure 1

3D geometric modeling of plain-woven CFRP

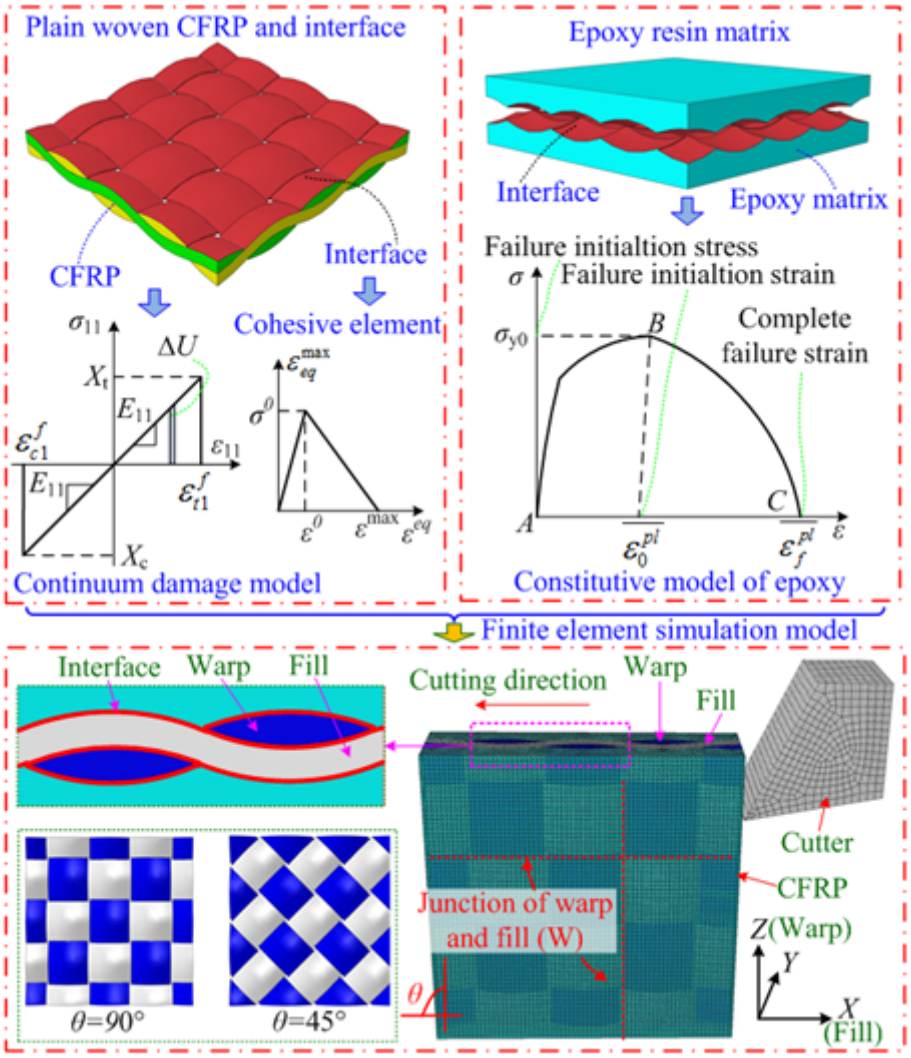

Figure 2

FEM modeling for plain-woven CFRP

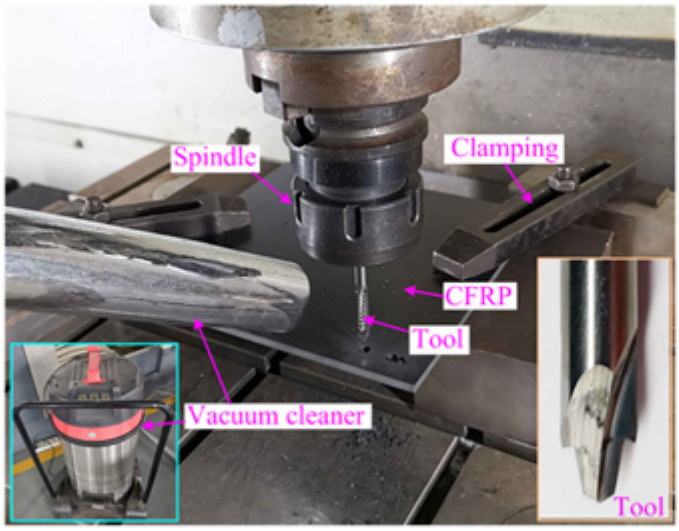

Figure 3

Experimental setups

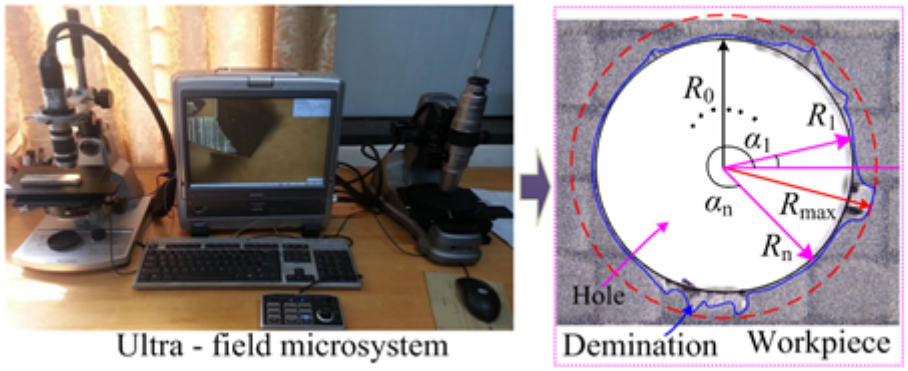

Figure 4

Measurement method for hole making delaminations

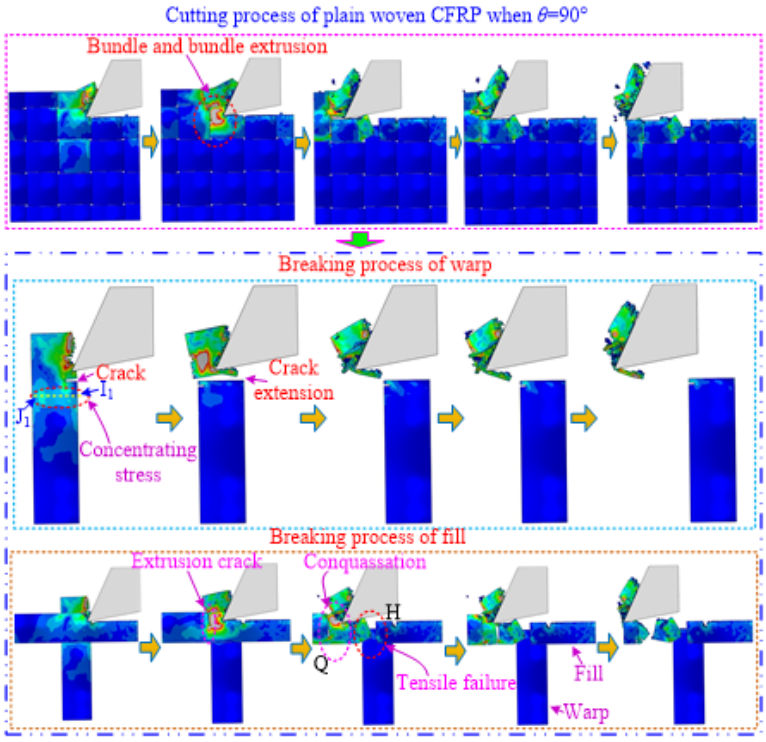

(a) Fiber bundles cutting process when θ=90°

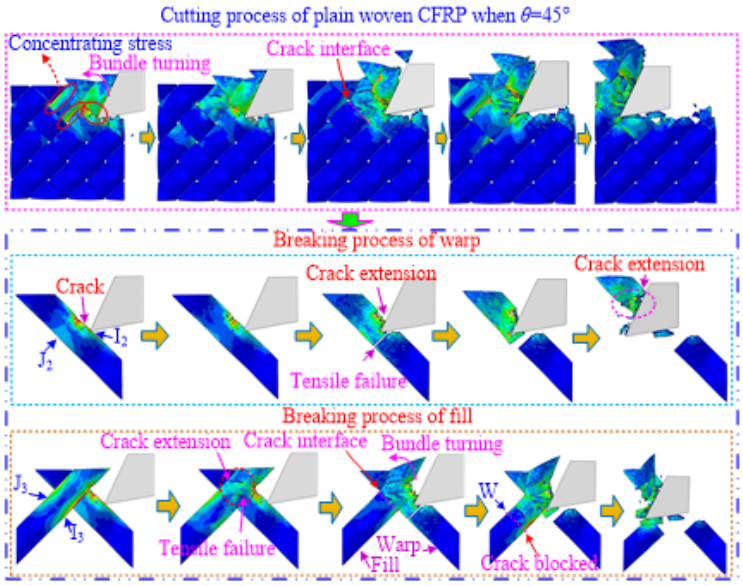

(b) Fiber bundles cutting process when θ=45°

Figure 5

Plain-woven fiber bundles cutting processes with different fiber orientation

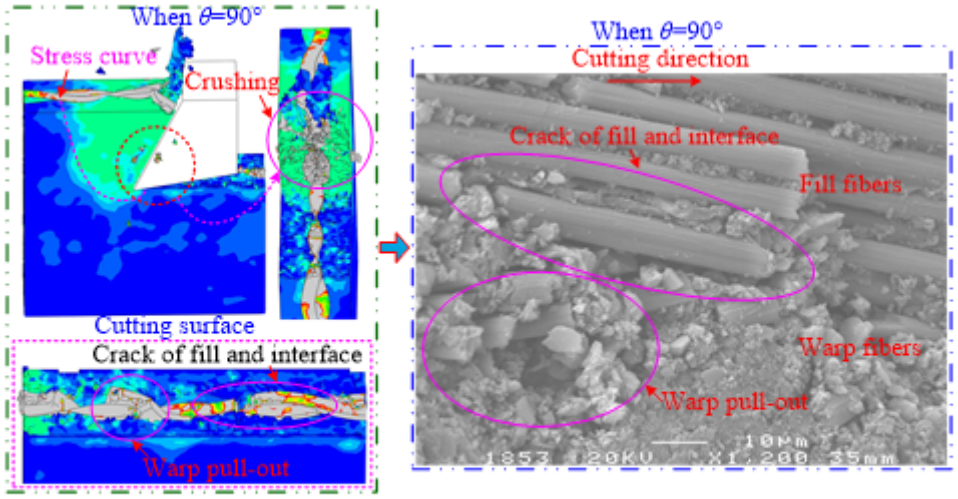

(a) Cutting surface when θ=90°

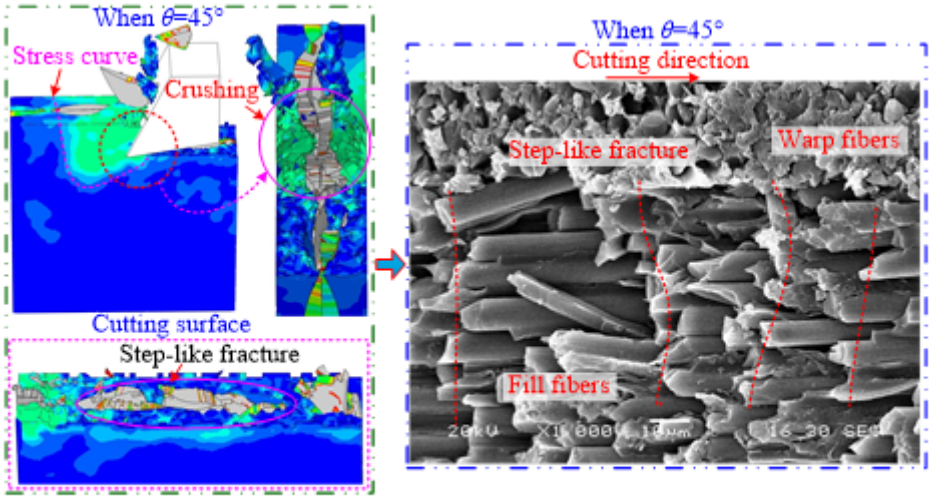

(b) Cutting surface when θ=45°

Figure 6

Plain-woven fiber bundles cutting surface with different warp fiber orientation

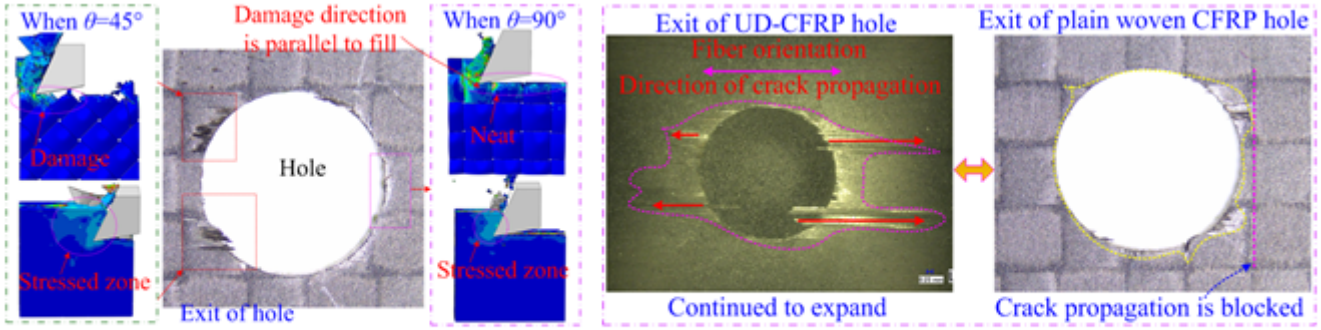

(a) Influence of plain-woven structure (b) Characteristics of hole making defects

Figure 7

Formation of manufactured defects

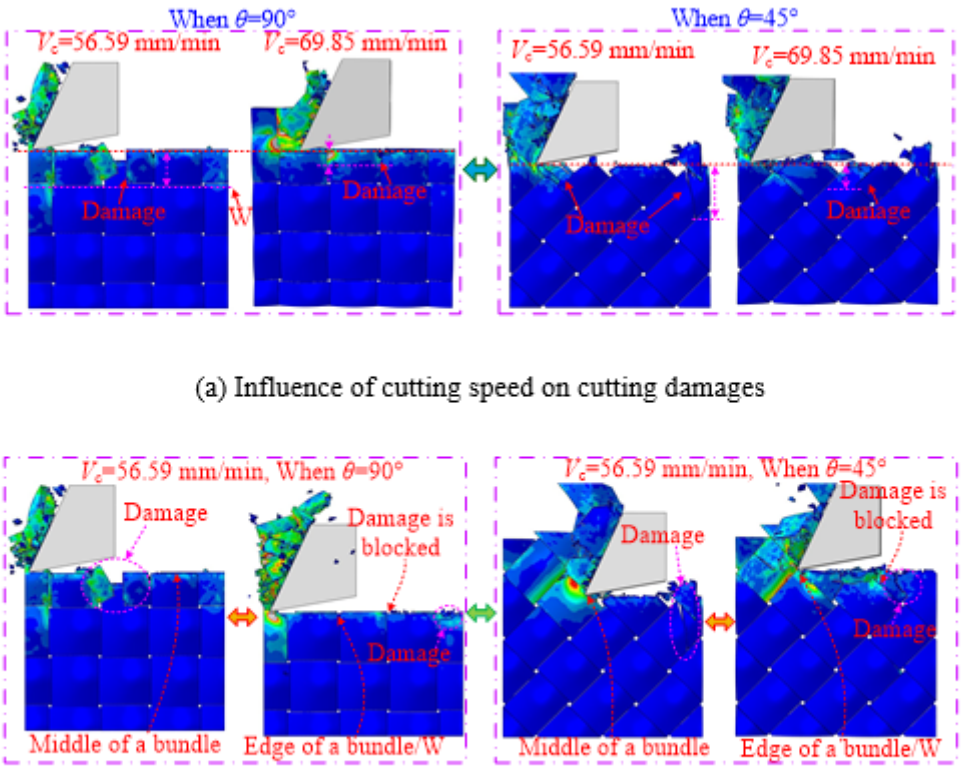

(a) Influence of cutting speed on cutting damages

(b) Influence of cutting point on cutting damages

Figure 8

Influences of cutting speed and cutting point on damages

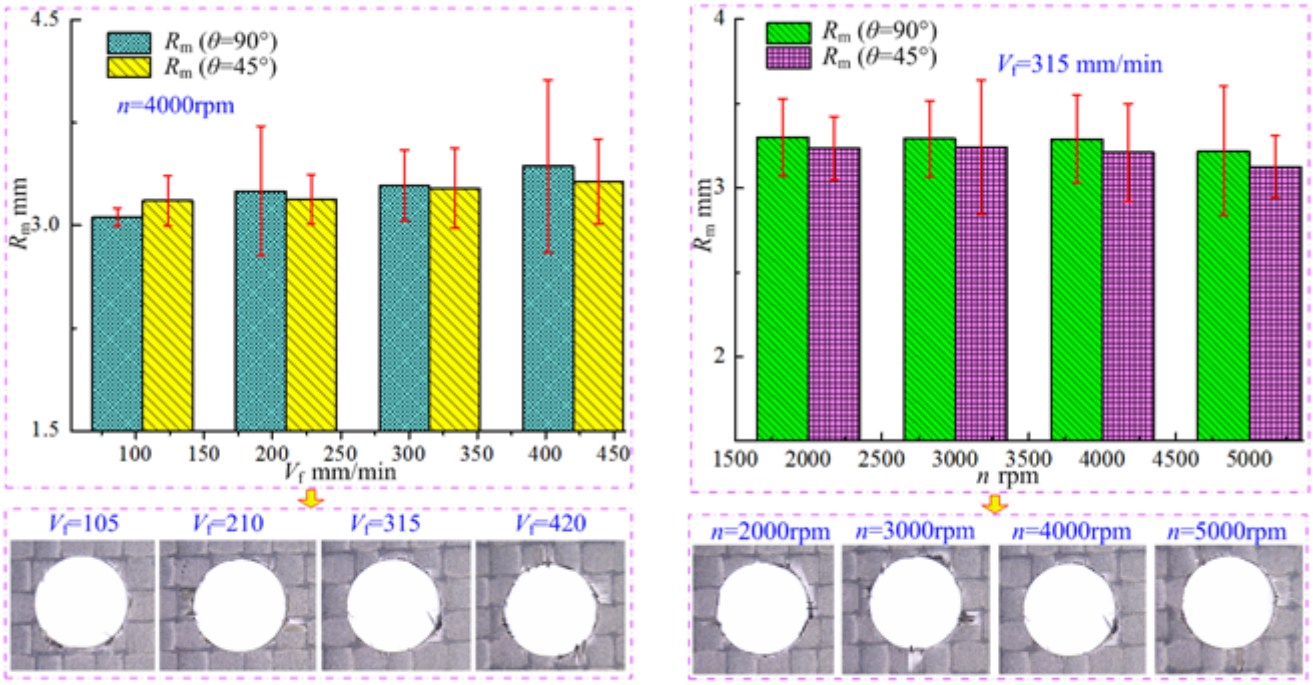

(a) Influence of feeding speed on delamination

(b) Influence of spindle speed on delamination

Figure 9

Influences of cutting parameters on delamination

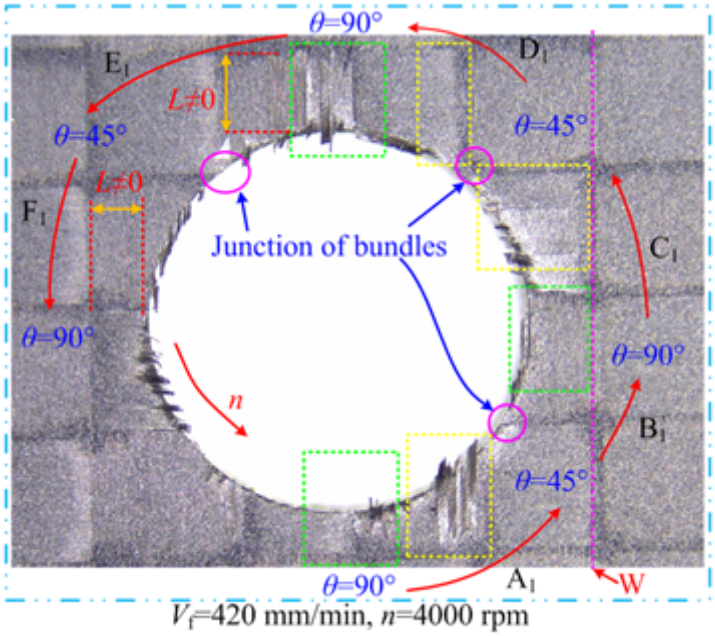

Figure 10

Evolutionary mechanism of plain-woven CFRP delaminations